Characterization of traditional artificial patinas on copper using the voltammetry of immobilized particles

Antonio Doménech-Carbó, Blanca Ramírez-Barat, Chiara Petiti, Sara Goidanich, María Teresa Doménech-Carbó, Emilio Cano

PII: S1572-6657(20)30721-9

DOI: https://doi.org/10.1016/j.jelechem.2020.114494

Reference: JEAC 114494

To appear in: *Journal of Electroanalytical Chemistry*

Received date: 16 April 2020

Revised date: 13 July 2020

Accepted date: 20 July 2020

Please cite this article as: A. Doménech-Carbó, B. Ramírez-Barat, C. Petiti, et al., Characterization of traditional artificial patinas on copper using the voltammetry of immobilized particles, *Journal of Electroanalytical Chemistry* (2020), https://doi.org/10.1016/j.jelechem.2020.114494

Characterization of traditional artificial patinas on copper using the voltammetry of immobilized particles

Antonio Doménech-Carbó*[a], Blanca Ramírez-Barat[b], Chiara Petiti[c], Sara Goidanich[c], María Teresa Doménech-Carbó[b], Emilio Cano[a],

[a] Departament de Química Analítica. Universitat de València. Dr. Moliner, 50, 46100 Burjassot (València) Spain.
[b] Centro Nacional de Investigaciones Metalúrgicas (CENIM), Consejo Superior de Investigaciones Científicas (CSIC), Avda. Gregorio del Amo 8, 28040 Madrid.
[c] Department of Chemistry, Materials and Chemical Engineering "Giulio Natta", Politecnico di Milano, P.za Leonardo da Vinci 32, 20133 Milano, Italy
[d] Institut de Restauració del Patrimoni. Universitat Politècnica de València. Camino de Vera 14, 46022, València, Spain.

* Corresponding autor. E-mail: antonio.domenech@uv.es.

Abstract

The voltammetry of immobilized particles methodology (VIMP) is used to characterize the composition of artificial patinas on copper. The voltammetric response of carbonate-, nitrate-, chloride-, sulfate-, and sulfide-based patinas is described using sub-microsamples attached to graphite electrodes in contact with different aqueous acetate buffer. Patina-characteristic voltammetric profiles are obtained for the different artificial patinas that can be recognized using the generalized Tafel analysis of the voltammetric curves. VIMP data could also provide layer-by-layer information about composition and compactness/crystallinity of the patinas for which a simplified theoretical modeling is presented.

Keywords: Electrochemistry; Artificial patinas; Copper; Bronze.

1. Introduction

Metal corrosion claims continuous interest because of its high scientific and technological importance, the research being mainly focused on corrosion inhibitors [1-6] and structure/composition of metal patinas and corrosion layers [7,8]. In this context, artificial patination, although practiced since the antiquity [9], is receiving increasing attention, mainly in order to better understand the mechanisms of formation of natural patinas, to test new conservation treatments and, to a lower extent, to better characterize artistic patinas [10-22]. Artistic patination was instead performed by artists for aesthetic reasons, conferring different colors and textures to the alloy surface. Artificial patination involves a variety of compounds, in particular those usually found in natural patinas (cuprite, Cu_2O, atacamite and its polymorphs, $Cu_2(OH)_3Cl$, copper hydroxysulfates, mainly brochantite, $Cu_4SO_4(OH)_6$, antlerite, $Cu_3SO_4(OH)_4$, and posnjakite, $Cu_4SO_4(OH)_6 \cdot H_2O$, copper hydroxycarbonates, malachite $Cu_2(OH)_2CO_3$, azurite, $Cu_3(OH)_2(CO_3)_2$, copper hydroxynitrate gerhardtite, $Cu_2(OH)_3(NO_3)$, but also nantokite, CuCl and tenorite, CuO and products of copper tarnishing, mainly chalcocite, Cu_2S and covellite, CuS) [22-24]. Tin and lead components also were used in artificial patination [25-27].

Traditional artificial patinas exhibit a significant variety in their structure and composition because of the proliferation of a number of recipes developed by individual workshops and the lack of detailed documentation about the manufacturing process [26,27]. The characterization of the components of artificially patinated cultural objects is an obvious analytical target for understanding their corrosion [28,29] and, consequently, for archaeometric, conservation and restoration purposes, including the detection of possible forgeries and/or artificial aging. This can be achieved by means of electron microscopy (SEM/EDX), x-ray diffraction (XRD), infrared (ATR-FTIR) and Raman spectroscopies, all well-established techniques for the study of natural patinas [30-32].

In order to complement the available techniques for the characterization of traditional artificial patinas, a study based on the voltammetry of immobilized particles methodology (VIMP) is here reported. This technique, developed by Scholz et al. [33], provides analytical information on a variety of sparingly soluble solids, as described in

recent reviews [34,35]. Due to its possibility of handling samples at the sub-microgram (nanogram, if necessary) level, the VIMP found application in the field of cultural heritage [36] and has been used to identify copper corrosion products [37-41] also with archaeometric purposes [42-44]. This technique was applied here to characterize artificial patinas prepared following different traditional recipes. This aim is of particular interest in the field of conservation and restoration of cultural heritage, where it is frequent to find objects that underwent to 'historic' but unknown patination procedures, with the concomitant difficulty of performing appropriate conservative tasks [9]. In this work, square wave voltammetry (SWV) was used as detection methodology for sample-modified paraffin-impregnated graphite electrodes immersed in aqueous acetate buffer at pH 4.75. This technique was combined with attenuated total reflectance-Fourier transform infrared spectroscopy (ATR-FTIR) in order to characterize the composition of a series of artificial patinas prepared on copper and bronze specimens. Our study is limited to chemical patination methods resulting in nitrate-, carbonate-, sulfate- and/or sulfide-based patinas applied over three metal substrates, copper, binary and ternary bronzes.

2. Experimental

Two sets of artificial patinas consisting of typical red, green and brown patinas on bronze were prepared by a foundry (Fonderia Artistica Battaglia, Milan, Italy) following traditional techniques from the XIX century [1]. In particular, patinas labeled as 103, 108, 201, 206 and 605 were produced by specialized craftsman of Fonderia Battaglia while patinas db, bbN1, bbN2, bbN3, 1.4, 1.72, and 1.117 were produced in the laboratory following traditional procedures. Moreover, patinas labeled as 2L, 4L, 6L and 8L were realized in laboratory with the aim of reproducing the surface conditions of an object that has been exposed to a chloride-rich environment by applying 2, 4, 6 and 8 layers of a paste constituted by CuCl plus $CuCl_2 \cdot 2H_2O$ plus $CuSO_4 \cdot 5H_2O$ paste. Table 1 summarizes the artificial patinas in this study. The details about their manufacturing are provided as a Supplementary Information, Tables S.1 and S.2. It is pertinent to note that, as judged by the standard potentials of the involved couples, most preparative processes would be no spontaneous under standard conditions. By this reason, most of the preparative processes involves heating above 100 ºC at air, conditions where copper

oxidation occurs without aqueous environment, far from the aforementioned standard conditions. The metal substrates were: A: Cu 90.55 %wt, Zn 2.34 %wt, Sn 6.14 %wt, Pb 0.97 %wt; B: binary bronze (Pb 95 %wt, Sn 5%wt); C: copper.

The preparation of some patinas (see Table 1) involved finishing treatments using a commercial wax (by Cera Novecento) constituted by bees wax and spirit of turpentine optionally in spray in trichloroethylene and/or commercial spray lake (alkyd varnish "Tinta RAL trasparente lucido" by Talken Color).

Voltammetric experiments were performed at sample-modified paraffin-impregnated graphite (Alpino HB, 2.0 mm diameter) electrodes using aqueous 0.25 M HAc/NaAc buffer at pH 4.75 as a supporting electrolyte. Measurements were carried out in a standard three-electrode cell connected to a CH I660 potentiostat, completed with a platinum auxiliary electrode and a Ag/AgCl (3M NaCl) reference electrode. Electrode conditioning was performed by abrasively pressing the edge of the graphite electrode onto the surface of the probes and then transferring the electrode into the electrochemical cell, as customary in VIMP experiments [24-26]. To mimic the experimental conditions operating in field analysis, no deaeration of the electrolyte was carried out.

ATR-FTIR experiments were carried out directly on the metallic coupons, using a Thermo Nicolet 6700 spectrophotometer with DTGS detector with detection range between 4000-400 cm^{-1}, equipped with a diamond window. The graphite electrode surfaces were examined using field emission scanning electron microscopy (Model S-4800, Hitachi Ltd., Tokyo, Japan) operating at 20 kV. The microanalysis of samples was performed with X-ray microanalysis system (SEM/EDX).

3. Results and discussion

3.1. Cuprite-based patina

A first set of measurements were performed on a *rosso* patina (108) that resulted constituted by a layer dominated by cuprite. Figure 1 shows the SWVs of sample modified-graphite electrodes in contact with air-saturated 0.25 M HAc/NaAc aqueous solution at pH 4.75 for patina 108. Upon scanning the potential from 0.65 V in the negative direction, a well-defined cathodic signal appears at ca. –0.15 V vs. Ag/AgCl

(C_1) followed by a cathodic wave at ca. –0.75 V (C_{ox}) which can be attributed to the reduction of dissolved oxygen (oxygen reduction reaction, ORR) as judged by blank experiments at unmodified graphite electrodes. The peak C_1 shows a shoulder in principle attributable to the existence of a wide distribution of shape and size of the cuprite grains, a frequent feature in VIMP [33-35]. In the subsequent positive-going voltammograms, a tall oxidation peak at ca. 0.05 V (A_1) is recorded. This corresponds to the stripping oxidation of the deposit of copper metal formed during the process C_1 to Cu^{2+} (aq).

The main component of the patina 108 is cuprite, as denoted by ATR-FTIR spectra and confirmed upon comparison of the voltammetric parameters with those of cuprite blanks, both displaying quite similar Tafel parameters (vide infra) [45,46]. The electrochemical reduction of cuprite can be represented as [38,39,42-44]:

$$Cu_2O_{(solid)} + 2H^+_{(aq)} + 2e^- \rightarrow 2Cu_{(solid)} + H_2O \quad (1)$$

This voltammetric response was reproduced in other red patinas, the light differences observed between them being attributable to differences in crystallinity and grain size, in turn resulting in minimal spectral differences [47-50].

3.2. Nitrate-based patinas

A second group of artificial patinas present gerhardtite ($Cu_2(OH)_3(NO_3)$) as a main constituent. This is a sparingly soluble compound with pK_s = 37.3 [51]. Figure 2 compares the SWVs of graphite electrodes modified with samples from patinas a,b) bb N1 and c,d) bb N2. The voltammetric response is similar to the patinas in Fig. 1, with a cathodic peak at ca. –0.15 V vs. Ag/AgCl (C_1) followed by the ORR wave at ca. –0.75 V (C_{ox}). In the positive-going voltammograms, a tall oxidation peak at ca. 0.00 V (A_1) is recorded. The voltammetry of patinas 201 and 206 was similar, but in those cases the peak C_1 appears resolved into two signals at 0.02 (C_{1a}) and –0.15 V (C_{1b}). This second signal is clearly enhanced after wax treatment, as can be seen on comparing Figs. 3a and 3c. This feature can be interpreted on assuming that the wax treatment results in a narrow distribution of crystallite sizes and hence in sharp voltammetric signals.

Voltammetric data can be correlated with ATR-FTIR spectra. Fig. 4 shows the spectra of the patina 206 before (a) and after (b) the application of a finishing treatment with wax. Both spectra display absorption bands at 3540, 1412, 1045, 870, 657 cm^{-1}, representative of gerhardite [52], accompanied by bands at 1290 and 749 cm^{-1} attributable to copper nitrate hydrate thanks to the comparison of a reference spectrum. The wax-treated patina produced the same bands but broadened and accompanied by the acute bands at 2918 and 2850 cm^{-1} which corresponds to the more prominent absorption bands of the wax [53].

Spectral data permit to identify gerhardtite, $Cu_2(NO_3)(OH)_2$, as the main component of the patina. Accordingly, the reduction process C_1 can be represented as the proton-assisted, two-electron reduction of this compound to copper metal:

$$Cu_2(NO_3)_2(OH)_{2\ (solid)} + 2H^+_{\ (aq)} + 4e^- \rightarrow 2Cu_{\ (solid)} + 2NO_3^-{}_{(aq)} + 2H_2O \quad (2)$$

The peak splitting appearing in this signal in several cases can be attributed to the differences in the crystallinity and shape and size of the gerhardtite crystals and/or the occurrence of similar reduction processes for other minority copper minerals such as rouaite (dimorph of gerhardtite), likasite ($Cu_3(OH)_5NO_3{\cdot}2H_2O$) or $Cu(NO_3)_2{\cdot}xH_2O$ which dissolves slowly:

$$Cu(NO_3)_2{\cdot}xH_2O_{\ (solid)} + 2e^- \rightarrow Cu_{\ (solid)} + 2NO_3^-{}_{(aq)} + xH_2O \quad (3)$$

3.3. Sulfide-based patinas

These are dark patinas prepared from $(NH_4)_2S$ or K_2S but also from K_2SO_4 under thermal stress. Figure 5 shows the voltammetric response (three replicate experiments) recorded for sample db. In the negative-going potential scan, well-defined reduction peaks at –0.15 V (C_1) and –0.55 V (C_2) appear preceding the C_{ox} wave, while in the positive-going scan, the stripping oxidation A_1 is followed by a broad anodic signal at ca. 0.20 V (A_2). On the basis of blank voltammograms for CuS (see Figure S.1 in Supplementary Information), this voltammetry can be rationalized on assuming the presence in the patina of copper sulfides, in principle consisting of a mixture of Cu_2S

(chalcocite) and CuS (covellite). Consistently, the patinas of this type do not produce well-defined IR spectra. Figure 6 depicts the CVs of graphite electrodes modified with sample 605 immersed when the potential is scanned between a) 0.65 V and –0.85 V and b) between 0.65 and –0.25 V. In the first case, the aforementioned signals C_1, C_2, A_1, A_2 are recorded accompanying the prominent C_{ox} process. The cathodic signals are preceded by a reduction peak at 0.25 V (C_3). When the potential range is restricted to the cathodic region in which the process C_1 appears, the process C_1 is not accompanied by a significant stripping oxidation A_1. In the anodic scan, the signal A_2 is resolved into waves at ca. 0.20 and 0.35 V. These voltammetric features can be interpreted on the basis of literature data [54,55], in terms of the stepwise reduction of CuS yielding Cu_2S via the process C_3:

$$2CuS_{(solid)} + 2H^+_{(aq)} + 2e^- \rightarrow Cu_2S_{(solid)} + H_2S \quad (4)$$

This compound would be further reduced to copper metal in the process C_1:

$$Cu_2S_{(solid)} + 2H^+_{(aq)} + 2e^- \rightarrow 2Cu_{(solid)} + H_2S \quad (5)$$

Our data, however, suggest that the cathodic process (C_2) can be attributed to the 'direct' reduction of covellite:

$$CuS_{(solid)} + 2H^+_{(aq)} + 2e^- \rightarrow Cu_{(solid)} + H_2S \quad (6)$$

As before, the anodic signal A_1 corresponds to the oxidation of the copper deposit to Cu^{2+} (aq), but the process A_2 can be attributed to the S-centered oxidation processes:

$$Cu_2S_{(solid)} \rightarrow 2Cu^+_{(aq)} + S + 2e^- \quad (7)$$

$$CuS_{(solid)} \rightarrow Cu^{2+}_{(aq)} + S + 2e^- \quad (8)$$

It is pertinent to note, however, that substoichiometric species can also be involved [54,55].

The above scheme is directly supported by CV experiments at different potential ranges. Interestingly, the green patina bb N2 deposited onto a first layer of sulfide patina presents a voltammetric profile where the copper sulfide and gerardhtite signals are superimposed. This is of interest in regard to the possible elucidation of the composition and structure of multi-layered patinas and ultimately studying artificial aging. As can be seen in Figure S.2 of Supplementary Information, in this case the ratio between the peak current of the signals C_1 and C_2 is close to one and the anodic region presents the peaks A_1 and A_2 with similar height.

3.4. Other patinas

An additional series of artificial patinas were prepared combining treatments with solutions of NaCl, NH_4Cl, and $CuSO_4$. Pertinent data are presented as a Supplementary Information, Table S.2 and Figure S.3. The voltammetric response is dominated by a cathodic signal at ca. –0.15 V (C_1) and the concomitant stripping oxidation at ca. 0.05 V (A_1). This voltammetric pattern is consistent with ATR-FTIR data in literature [56-58]. The spectra of these patinas (Figure S.4, Supplementary Information) show atacamite bands at 3340, 3323, and at low frequencies between 983 and 510 cm^{-1}, accompanied by the band ca. 3170 and 1055 cm^{-1}, due to the presence of non-reacted $CuSO_4$ hydrate [56-58]. These features indicate the formation of atacamite as a main component of the patinas prepared from chloride-containing solutions. Interestingly, in several cases, the profile of the stripping peaks for copper oxidation becomes highly characteristic. This feature, which is to some extent surprising, results from the different shape and size distribution of the deposit of metallic copper formed in the reduction of the parent copper components of the respective patina and the possible complexation of Cu^{2+} ions produced in the stripping process by the anionic species (Cl^-, NO_3^-, SO_4^{2-}, etc.) released during the cathodic steps. Figure S.5 in Supplementary information contains some representative anodic profiles.

3.5. Layer-by-layer analysis

Voltammetric data can provide information of the in-depth composition of the patina. In principle, and given the stepped nature of the manufacturing procedures (see Supplementary Information, Table S.1), it is reasonable to expect that the composition of the patina varies in depth, as occurring for natural patinas [59,60] and/or varies in the crystallinity of the components. For the purpose of layer-by-layer analysis, different

pressures were applied to the graphite bar when sampling the patinas over the metallic specimens. This method differs from that previously reported, based on successive voltammetric records [61], which involves the immersion of the metal object into an electrolyte.

The sampling process, consisting of pressing the graphite electrode onto the patina, is schematized in Figure 7a. On increasing the pressure of the graphite bar, a set of micrometer-sized fragments of the patina become adhered onto the graphite as can be seen in the SEM image in Figure 7b. The patina laminas (characterized by its Cu content determined by EDX) become irregularly distributed over the graphite surface. On increasing the pressure of the bar, one can expect that the number and size of removed fragments increase.

Figure 8 depicts five negative-going potential scan voltammograms after sampling with different pressures for a) gerardhtite patina 108, and b) chloride and sulfate patina 6L. In the both cases, the cathodic signal C_1 increases on increasing the pressure exerted by the graphite bar on the patina during the sampling process, thus denoting that there is an increase in the net amount of sample transferred to the graphite surface. In the case of the gerardhtite patina 108 at low sample amounts, the voltammogram consists of a main cathodic peak at ca. −0.05 V (C_{1a}) which is accompanied by a shoulder at −0.15 V (C_{1b}). Upon increasing the amount of sample, this second signal increases so that the voltammetric pattern moves from one peak to a two-peak profile. In contrast, the voltammograms of the chloride and sulfate patina 6L is dominated by the signal C_{1b} which increases on increasing the amount of sample transferred onto the graphite electrode.

These features can be interpreted on assuming that, as characterized for natural corrosion patinas [50,52], there is a primary compact 'impermeable' patina of defective cuprite covered by a less compact, 'permeable' patina of cuprite and/or other components. In the case of cuprite patinas, when 'smooth' sampling is performed, the voltammogram reflects the composition of the external, less compact patina which would be responsible for the signal C_{1a}. When 'hard' sampling is carried out, the voltammogram is dominated by the voltammetric signal C_{1b}, produced by the compact patina. For other than cuprite patinas, however, the cathodic signals can reflect more

complex gradients of composition and compactness/crystallinity so that the intensity of peaks C_{1a}, C_{1b} reflect the respective amounts of two different species having different composition and/or compactness, porosity, etc. The appearance of two reduction peaks attributed to different crystallinity of cuprite has also been observed by other authors in laboratory produced patinas [62,63]

Figure 9 represents the values of the ratio between the signals at more positive (C_{1a}) and more negative (C_{1b}) potentials, $i(C_{1a})/i(C_{1b})$, vs. the sum of these signals, $i(C_{1tot})$ (= $i(C_{1a}) + i(C_{1b})$), for several patinas in this study. Since the impermeable patina can be assumed to be deeper, the $i(C_{1a})/i(C_{1b})$ ratio is representative of the ratio between the averaged amounts of the components responsible for peaks C_{1a} and C_{1b} while $i(C_{1tot})$ is representative of the net amount of sample extracted from the patina.

As can be seen in Figure 9, the cuprite (108), sulfide (605), and chloride (6L) patinas display a similar slightly decreasing variation of $i(C_{1a})/i(C_{1b})$, on $i(C_{1tot})$. In contrast, the nitrate patina 201 shows an increasing variation of $i(C_{1a})/i(C_{1b})$, on $i(C_{1tot})$. To rationalize these features, it is possible to formulate a theoretical model assuming that the voltammetric currents $i(C_{1a})$ and $i(C_{1b})$ are proportional to the amount of the respective 'permeable' (a) and 'impermeable' (b) components which proportion varies continuously through the patina. The variation in the shape of the voltammetric signatures with the pressure exerted in the sampling process suggests that not only the number of patina fragments but also the depth reached in the sampling varies. In the following, we adopt a highly idealized model assuming that the graphite bar extracts a set of N identical circular laminas of radius r and depth z ($z << r$) from the external patina. Then, the net amount m_j of sample of the j-component (j = a,b) transferred from the specimen to the graphite bar can be approximated by:

$$m_j = \int_{z=0}^{z} N\pi r^2 \delta\rho_j(z)dz \qquad (9)$$

where $\rho_j(z)$ represents the depth-dependent density of the j-component forming the patina.

We assume that there is a monotonical variation with depth of the density of the a-component (responsible for peak C_{1a}) and the density of the b-component (responsible for peak C_{1b}). The former will decrease from a surface value, ρ_a^{sup}, while the second should increase concomitantly until a certain limiting value, ρ_b^{inf}. Although there are different possible $\rho(z)$ functions, potential ones are particularly interesting due to its flexibility to reproduce large or small density gradients. Previous studies on natural patinas on coins permitted to correlate satisfactorily concentration gradients determined by EDX in the patina and voltammetric data with this type of functions [42,43]. Accordingly, the expressions for the in depth variation of the densities of the a- and b-components of the patina can be written as:

$$\rho_a(z) = \rho_a^{sup}\left[1-(z/z_o)^{\alpha}\right] \qquad (10)$$

$$\rho_b(z) = \rho_b^{inf} - \rho_a^{sup}\left[1-(z/z_o)^{\beta}\right] \qquad (11)$$

where z_o represents the depth at which the b-component reaches its limiting density, ρ_b^{inf} and $\rho_a(z) = 0$. These functions accomplish the conditions $\rho_a(z) = \rho_a^{sup}$ when z = 0 and $\rho_b(z) = \rho_b^{inf}$ when $z = z_o$. In the above equations, α, β, are the exponents of the potential functions characterizing the variation of density of those components with depth. Introducing the electrochemical coefficient of response g_{1j}, the current measured for the a- and b-components will be:

$$i(C_{1a}) = \int_{z=0}^{z} Ng_{1a}\pi r^2 \rho_a^{sup}\left(1-\left(\frac{z}{z_o}\right)^{\alpha}\right)dz \qquad (12)$$

$$i(C_{1b}) = \int_{z=0}^{z} Ng_{1b}\pi r^2 \left[\rho_b^{inf} - \rho_a^{sup}\left(1-\left(\frac{z}{z_o}\right)^{\beta}\right)\right]dz \qquad (13)$$

Notice that the g_{1j} coefficients depend on the electrochemical conditions (potential scan rate, etc.) and the molar mass of the component (a, b). Integration of the above equations yield:

$$i(C_{1a}) = Ng_{1a}\pi r^2 \rho_a^{sup}\left(z - \frac{z^{1+\alpha}}{(1+\alpha)z_o^{\alpha}}\right) \qquad (14)$$

$$i(\mathrm{C}_{1b}) = Ng_{1b}\pi r^2\left[\rho_b^{inf} z - \rho_a^{sup}\left(z - \frac{z^{1+\beta}}{(1+\alpha)z_o^{\beta}}\right)\right] \qquad (15)$$

The total current will be the sum of $i(\mathrm{C}_{1a})$ plus $i(\mathrm{C}_{1b})$. Taking $g_{1a} \approx g_{1b} \approx: g_1$, one obtains:

$$i(\mathrm{C}_{1tot}) = Ng_1\pi r^2\rho_b^{inf} z \qquad (16)$$

It is pertinent to note that not only z, but also N and r will vary from one experiment to another. However, the $i(\mathrm{C}_{1a})/i(\mathrm{C}_{1b})$ ratio will be solely z-dependent:

$$\frac{i(\mathrm{C}_{1a})}{i(\mathrm{C}_{1b})} = \frac{g_{1a}}{g_{1b}}\frac{\rho_a^{sup}\left(z - \frac{z^{1+\alpha}}{(1+\alpha)z_o^{\alpha}}\right)}{\rho_b^{inf} z - \rho_a^{sup}\left(z - \frac{z^{1+\beta}}{(1+\beta)z_o^{\beta}}\right)} \qquad (17)$$

Since $z = i(\mathrm{C}_{1tot})/Ng_1\pi r^2\rho_b^{inf}$, the $i(\mathrm{C}_{1a})/i(\mathrm{C}_{1b})$ ratio can be expressed as a function of $i(\mathrm{C}_{1tot})$, taking $g_{1a} \approx g_{1b} \approx: g_1$, as:

$$\frac{i(\mathrm{C}_{1a})}{i(\mathrm{C}_{1b})} \approx \frac{\rho_a^{sup}\left(1 - \frac{i(\mathrm{C}_{1tot})^{\alpha}}{(1+\alpha)Ng_1\pi r^2\rho_b^{inf} z_o^{\alpha}}\right)}{\rho_b^{inf} - \rho_a^{sup}\left(1 - \frac{i(\mathrm{C}_{1tot})^{\beta}}{(1+\beta)Ng_1\pi r^2\rho_b^{inf} z_o^{\beta}}\right)} \qquad (18)$$

For the moderate pressures exerted during the sampling process, one can expect (see Fig. 7b) that the graphite bar removes fragments of (relatively) weakly bound external laminas of the (partially delaminated) metal corrosion patina. Then, increasing pressure should in principle result in an increase in the depth of the de-laminated fragments able to be extracted. Conceivably (see Supplementary information, Fig. S.7), increasing sampling pressure determines an increase of the fragmentation so that the number of removed patina particles increase while their average radius decreases. Accordingly, the Nr^2 product can be taken as approximately constant so that Eq. (18) predicts a polynomial variation of $i(\mathrm{C}_{1a})/i(\mathrm{C}_{1b})$, on $i(\mathrm{C}_{1tot})$. This variation depends on the

parameters α, β, z_o, ρ_a^{sup}, ρ_b^{inf}, characterizing the composition and/or compaction/crystallinity of the patina and its in-depth distribution. Although this model contains several adjustable parameters whose estimate is uncertain in several cases, these can be grouped into two coefficients, $1/(1+\alpha)Ng_1\pi r^2\rho_b^{inf}z_o^{\alpha}$, and $1/(1+b)Ng_1\pi r^2\rho_b^{inf}z_o^{\beta}$, whose value has to be similar. Consistently, experimental data in Figure 9 can be fitted to Eq. (18) using the values of the densities of the minerals constituting the main component of each patina and similar values of these coefficients (including α and β exponents). Table 2 summarizes the values of the above parameters for patinas 108 (cuprite type), 201 (nitrate type), 605 (sulfide type), and 6L (chloride type). Patinas 108, 605 and 6L yield a decrease of $i(C_{1a})/i(C_{1b})$ on increasing $i(C_{1tot})$ which can be directly fitted to Eq. (18). In contrast, patina 201 displays the opposite behavior, the ratio $i(C_{1a})/i(C_{1b})$ increasing on increasing $i(C_{1tot})$. This can easily be modeled simply interchanging the equations for the a- and b-components. Table 2 shows the corresponding parameters.

3.6. Tafel analysis

Since the voltammetric response of the majority of copper corrosion products of natural and artificial patinas is very similar, Tafel analysis of the voltammetric curves provides, a valid method to discriminate the different compounds [45,46,57]. The Tafel plots of the logarithm of the ratio between the current i at a potential E and the peak current, i_p, vs. the difference between E and the peak current, E_p, for different sampling performed on patinas a) 108 and b) 201 is provided as a Supplementary information, Figure S.6. This analysis was made taking current/potential measurements at potentials between 125 and 250 mV more positive than the peak potential of the voltammetric signal. The plots of $\ln(i/i_p)$ vs. $E–E_p$ for negative-going potential scan voltammograms such as in Figure 8 yield practically parallel straight lines whose ordinate at the origin varies within a relatively narrow range in the case of the patina 108 and becomes almost the same for patina 201.

Figure 10 depicts the two-dimensional diagram containing the values of the slope (*SL*) and the ordinate at the origin (*OO*) of Tafel plots determined from replicate voltammetric experiments on artificial patinas in this study. It can be observed that the values related to nitrate-, chloride plus sulfate- and cuprite-based patinas are

concentrated in more or less separated regions, roughly along a diagonal line. The points of sulfide-based patinas, instead, fall in a clearly separated region of the diagram. The data points for each patina, however, fall within relatively extended regions of the diagram. This feature can be interpreted in the light of our previous study on the characterization of copper and lead corrosion products on leaded bronze statuary by means of Tafel analysis [64]. The essential idea is that, due to the insulating or semiconducting nature of the components of the patinas, they produce a more or less large uncompensated ohmic drop in the electrochemical cell depending on the net amount of sample transferred onto the electrode surface. The incorporation of such uncompensated ohmic drops into the Tafel equation yields [64]:

$$\ln\left(\frac{i}{i_{\mathrm{p}}}\right) = H + G(R_{\Omega}) - \frac{\alpha n F}{RT}(E - E_{\mathrm{p}}) \qquad (18)$$

where H represents the Tafel ordinate at the origin in the absence of uncompensated ohmic effects and $G(R_{\Omega})$ is a term depending, among other factors, on the uncompensated ohmic resistance, R_{Ω}, and the other symbols have their usual meaning. This means that for a series of samples with different R_{Ω} values the Tafel representations will present essentially the same slope but different ordinate at the origin. This can be seen in the Tafel plots in Figure S.6 and is reflected in the dispersion observed in the (Tafel slope)/(Tafel ordinate at the origin) two-dimensional diagram in Figure 10. This diagram illustrates the possibility of discriminating between different artificial patinas by VIMP using sub-microsamples. It has to be underlined that the discrimination of patinas by means of VIMP may be of great interest in the cultural heritage field. It allows characterizing and distinguishing copper compounds with a micro-invasive approach, even when other micro-invasive or non-invasive techniques (e.g. ATR-FTIR) result ineffective in detecting some of the minerals contained in the artificial patinas or corrosion layers.

4. Conclusions

The voltammetric response of a series of artificial patinas prepared according to traditional recipes on copper and bronze substrates has been studied using the voltammetry of immobilized particles methodology. The square wave voltammograms of sub-microsamples extracted from artificial patinas on copper and bronze consists, in contact with aqueous acetate buffer at pH 4.75, of well-defined cathodic signals due to the reduction of the copper compounds forming the protective patina. Voltammetric data, supported by ATR-FTIR spectroscopy permits to characterize gerardhtite as the main component in patinas prepared from nitrate, atacamite accompanied by copper sulfate hydrate in the patinas prepared from chloride plus sulfate baths, whereas sulfide-based treatments present a thin patina with chalcocite. Other preparative recipes produce cuprite patinas.

The modulation of the pressure exerted by graphite electrodes on the patinas allows to obtain layer-by-layer information on the composition and compactness/compaction of the patinas using the depth variation of voltammetric parameters. This variation can be modeled using a simple description of the distribution of the components of the patina in depth. The different patinas can be characterized and distinguished using the Tafel plots from current-potential curves in the foot of the voltammetric signals resulting from the negative-going potentials scans, related to the reduction of copper compounds. The possibility of characterizing and distinguishing the artificial patinas on an electrochemical basis, with a submicro-invasive approach can be of great interest for conservation and restoration purposes, thus expanding the potentialities of the voltammetry of immobilized particles in this field.

Acknowledgments: Authors gratefully acknowledge funding from Project CTQ2017-85317-C2-1-P, supported with *Ministerio de Economía, Industria y Competitividad* (MINECO), *Fondo Europeo de Desarrollo Regional* (ERDF) and *Agencia Estatal de Investigación* (AEI); and project TOP-HERITAGE CM (S2018/NMT_4372) from Comunidad de Madrid and European Structural and Investment Funds. B. R.-B. and E.C. would like to professional support of the CSIC Interdisciplinary Thematic Platform “Open Heritage: Research and Society” (PTI-PAIS).

References

[1] J. Telegdi, T. Rigó, E. Kálmán, Molecular layers of hydroxamic acids in copper corrosion inhibition, J. Electroanal. Chem. 582 (2005) 191–201.

[2] F. Caprioli, F. Decker, V. Di Castro, Durable Cu corrosion inhibition in acidic solution by SAMs of Benzenethiol, J. Electroanal. Chem. 657 (2011) 192–195.

[3] S. Neodo, D. Carugo, J.A. Warthon, K.R. Stokes, Electrochemical behaviour of nickel-aluminium bronze in chloride media: Influence of pH and benzotriazole, J. Electroanal. Chem. 695 (2013) 38–46.

[4] A. Romeiro, C. Gouveia-Caridade, C.M.A. Brett, Polyhenazine films as inhibitors of copper corrosion, J. Electroanal. Chem. 688 (2013) 282–288.

[5] K. Krishnaveni, J. Ravichandran, Influence of aqueous extract of leaves of Morinda tinctoria on copper corrosion in HCl medium, J. Electroanal. Chem. 735 (2014) 24–31.

[6] C. Rahal, M. Masmoudi, R. Abdelhedi, R. Sabot, M. Jeannin, M. Bouaziz, P. Refait, Olive leaf extract as natural corrosion inhibitor for pure copper in 0.5 M NaCl solution. A study of voltammetry around OCP, J. Electroanal. Chem. 769 (2016) 53–61.

[7] G. Bertrand, E. Rocca, C. Savall, C. Rapin, J.-C. Labrune, P. Steinmetz, In-situ electrochemical atomic force microscopy studies of aqueous corrosion and inhibition of copper, J. Electroanal. Chem. 489 (2000) 38–45.

[8] A. Xu, C. Dong, X. Wei, X. Li, D.D. Macdonald, DFT and photoelectrochemical studies of point defects in passive films on copper, J. Electroanal. Chem. 834 (2019) 216–222.

[9] R. Hughes, M. Rowe, The Colouring Bronzing and Patination of Metals, Thames & Hudson, London (GB), 1991.

[10] P. Dillmann, G. Beranger, P. Piccardo, H. Matthiessen, Corrosion of MetallicHeritage Artefacts, Investigation, Conservation and Prediction for Long-term Behaviour, Woodhead Pub., Cambridge (GB), 2007 (EFC publications (EFC48)).

[11] T. Beldjoudi, F. Bardet, N. Lacoudre, S. Andrieu, A. Adriaens, I. Constantinides, P. Brunella, Surface modification processes on European union bronze reference materials for analytical studies of cultural artifacts, Surf. Eng. 17 (2001) 231–235.

[12] I. Constantinides, A. Adriaens, F. Adams, Surface characterization of artificial corrosion layers on copper alloys reference materials, Appl. Surf. Sci. 189 (2002) 90–101.

[13] G. Di Carlo, C. Giuliani, C. Riccucci, M. Pascucci, E. Messina, G. Fierro, et al. Artificial patina formation onto copper-based alloys: Chloride and sulphate induced corrosion processes, Appl. Surf. Sci. 421 (2017) 120–127.

[13] K.P. Fitzgerald, J. Nairn, A. Atrens, The chemistry of copper patination, Corros. Sci. 40 (1998) 2029–2050.

[14] G. Masi, J. Esvan, C. Josse, C. Chiavari, E. Bernardi, C. Martini, et al. Characterization of typical patinas simulating bronze corrosion in outdoor conditions, Mat. Chem. Phys. 200 (2017) 308–321.

[15] K. Marušić, H. Otmačić-Ćurković, Š. Horvat-Kurbegović, H. Takenouti, E. Stupnišek-Lisac, Comparative studies of chemical and electrochemical preparation of artificial bronze patinas and their protection by corrosion inhibitor, Electrochim. Acta. 54 (2009) 7106–7113.

[16] T. Kosec, H.O. Kurkovic, A. Legat, Investigation of the corrosion protection of chemically and electrochemically formed patinas on recent bronze, Electrochim. Acta 56 (2010) 722–731.

[17] B.M. Rosales, R.M. Vera, J.P. Hidalgo, Characterisation and properties of synthetic patina on copper base sculptural alloys, Corros. Sci. 52 (2010) 3212–3224.

[18] J. Muller, G. Lorang, E. Leroy, B. Laik, I. Guillot, Electrochemically synthesised bronze patina: characterisation and application to the cultural heritage, Corros. Eng. Sci. Technol. 45 (2013) 322–326.

[19] B.M. Rosales, R. Vera, G. Moriena, Evaluation Of The Protective Properties Of Natural And Artifcial Patinas On Copper. Part I. Patinas Formed By Immersion., Corros. Sci. 41 (1999) 625–651.

[20] A. Casanova Municchia, F. Bellatreccia, G. D'Ercoli, S. Lo Mastro, I. Reho, M.A. Ricci et al. Characterisation of artificial patinas on bronze sculptures of the Carlo Bilotti Museum (Rome), Appl. Phys. A 122(2016) 79–86.

[21] V. Hayez, T. Segato, A. Hubin, H. Terryn, Study of copper nitrate-based patinas. J. Raman Spectrosc. 37 (2006) 1211–1220.

[22] V. Hayez, V. Costa, J. Guillaume, H. Terryn, A. Hubin, Micro Raman spectroscopy used for the study of corrosion products on copper alloys: study of the chemical composition of artificial patinas used for restoration purposes, Analyst. 130 (2005) 550–556.

[23] E. Cano, J.L. Polo, A. La Iglesia, J.M. Bastidas, Rate control for copper tarnishing, Corros. Sci. 47 (2005) 977–987.

[24] G. Di Carlo, C. Giuliani, C. Riccucci, M. Pascucci, E. Messina, G. Fierro, M. Lavorgna, G.M. Ingo, Artificial patina formation onto copper-based alloys: Chloride and sulphate induced corrosion processes, Appl. Surf. Sci. 421 (2017) 120–127.

[25] E. Formigli, G. Lahusen, D. Ferro, Note di storia del restauro archeologico: i restauri settecenteschi ai grandi bronzi di Ercolano, KERMES: la rivista del restauro 18 (2005) 35–48.

[26] E. Formigli, D. Ferro, S. Bovani, La patina artificiale antica dei grandi bronzi di Ercolano, KERMES: la rivista del restauro 19 (2006) 29–34.

[27] I. Donate, M.C. Medina, R. Faceta, J. Barrio, A. Doménech-Carbó, A. Fuentes, A.I. Pardo, O. Martínez, Estudio interdisciplinar de pátinas en esculturas romanas de bronce procedentes del yacimiento de Valeria (Cuenca) in Proc. Metal España 2015, Segovia, Spain.

[28] M.C. Bernard, S. Joiret, Understanding corrosion of ancient metals for the conservation of cultural heritage, Electrochim. Acta 54 (2009) 5199–5205.

[29] B.M. Rosales, R.M. Vera, J.P. Hidalgo, Characterisation and properties of synthetic patina on copper base sculptural alloys, Corros. Sci. 52 (2010) 3212–3224.

[30] E. Franceschi, P. Letardi, G. Luciano, Colour measurements on patinas and coating system for outdoor bronze monuments, J. Cult. Herit. 7 (2006)166–170.

[31] C. Chiavari, K. Rahmouni, H. Takenouti, S. Joiret, P. Vermaut, L. Robbiola, Composition and electrochemical properties of natural patinas of outdoor bronze monuments, Electrochim. Acta 52 (2007) 7760–7769.

[32] S. Goidanich, J. Brunk, G. Herting, M.A. Arenas, I. Odnevall Wallinder, Atmospheric corrosion of brass in outdoor applications Patina evolution, metal release and aesthetic appearance at urban exposure conditions, Sci. Total Environ. 412–413 (2011) 46–57.

[33] F. Scholz, B. Meyer, B. Voltammetry of solid microparticles immobilized on electrode surfaces, Electroanalytical Chemistry, A Series of Advances, A.J. Bard, I. Rubinstein, Eds., Marcel Dekker, New York, 1998, vol. 20, pp. 1–86.

[34] F. Scholz, U. Schröder, R. Gulabowski, A. Doménech-Carbó, Electrochemistry of Immobilized Particles and Droplets, 2nd edit. Springer, Berlin-Heidelberg, 2014.

[35] A. Doménech-Carbó, J. Labuda, F. Scholz, Electroanalytical chemistry for the analysis of solids: characterization and classification (IUPAC Technical Report), Pure Appl. Chem. 85 (2013) 609–631.

[36] A. Doménech-Carbó, M.T. Doménech-Carbó, V. Costa, Electrochemical Methods in Archaeometry, Conservation and Restoration, Monographs in Electrochemistry Series, F. Scholz, Edit. Springer, Berlin-Heidelberg, 2009.

[37] V. Costa, K. Leyssens, A. Adriaens, N. Richard, F. Scholz, Electrochemistry reveals archaeological materials, J. Solid State Electrochem. 14 (2010) 449–451.

[38] D. Satovic, S. Martinez, A. Bobrowski, Electrochemical identification of corrosion products on historical and archaeological bronzes using the voltammetry of micro-particles attached to a carbon paste electrode, Talanta 81 (2010) 1760–1765.

[39] F. Arjmand, A. Adriaens, Electrochemical quantification of copper-based alloys

using voltammetry of microparticles: optimization of the experimental conditions, J. Solid State Electrochem. 16 (2012) 535–543.

[40] N. Souissi, L. Bousselmi, S. Khosrof, E. Triki, Electrochemical and spectroscopic characterizations of patinas formed on an archaeological bronze coin, Mater. Corros. 55 (2004) 284–292.

[41] M. Serghini-Idrissi, M. C. Bernard, F. Z. Harrif, S. Joiret, K. Rahmouni, A. Srhiri, H. Takenouti, V. Vivier, M. Ziani, Electrochemical and spectroscopic characterizations of patinas formed on an archaeological bronze coin, Electrochim. Acta 50 (2005) 4699–4709.

[42] A. Doménech-Carbó, M. T. Doménech-Carbó, E. Montagna, C. Álvarez-Romero, Y. Lee, Electrochemical discrimination of mints: the last Chinese emperors Kuang Hsü and Hsüan T'ung monetary unification, Talanta 169 (2017) 50–56.

[43] A. Doménech-Carbó, M.T. Doménech-Carbó, C. Álvarez-Romero, N. Montoya, T. Pasíes-Oviedo, M. Buendía-Ortuño, Electrochemical characterization of coinage techniques the 17th century: The *maravedís* case, Electroanalysis 29 (2017) 2008–2018.

[44] A. Doménech-Carbó, M.T. Doménech-Carbó, S. Capelo, T. Pasíes-Oviedo, I. Martínez-Lázaro, Dating archaeological copper/bronze artifacts using the voltammetry of microparticles, Angew. Chem. Int. Ed. 53 (2014) 9262–9265.

[45] A. Doménech-Carbó, M.T. Doménech-Carbó, H.G.M. Edwards, Application of Tafel analysis for quantitation in solid state voltammetry. Application to the analysis of cobalt and copper pigments in severely damaged frescoes, Anal. Chem. 80 (2008) 2704–2716.

[46] A. Doménech-Carbó, M.T. Doménech-Carbó, T. Pasíes-Oviedo, M.C. Bouzas-Bello, Application of modified Tafel analysis to the identification of corrosion products on archaeological metals using voltammetry of microparticles, Electroanalysis, 23 (2011) 2803–2812.

[47] G. Niaura, Surface-enhanced Raman spectroscopic observation of two kinds of adsorbed OH^- ions at copper electrode, Electrochim. Acta 45 (2000) 3507−3519.

[48] E. Basso, C. Invernizzi, M. Malagodi, M.F. La Russa, D. Bersani, P.P. Lottici, Characterization of colorants and opacifiers in roman glass mosaic tesserae through spectroscopic and spectrometric techniques, J. Raman Spectrosc. 45 (2014) 238−245.

[49] C.J. Keturakis, B. Notis, A. Blenheim, A.C. Miller, R. Pafchek, M.R. Notis, I.E. Wachs, Analysis of corrosion layers in ancient Roman silver coins with high resolution surface spectroscopic techniques, Appl. Surf. Sci. 376 (2016) 241–251.

[50] H. Stein, D. Naujoks, D. Grochla, C. Khare, R. Gutowski, S. Grützke, W. Schuhmann, A. Ludwig, A structure zone diagram obtained by simultaneous deposition on a novel step heater: A case study for Cu_2O thin films, Phys. Status Solidi A 212 (2015) 2798−2804.

[51] C.H. Yoder, E. Bushong, X. Liu, V. Weidner, P. McWilliams, K. Martin, J. Lorgunpai, J. Haller, R.W. Schaeffer, The synthesis and solubility of the copper hydroxyl nitrates: gerhardtite, rouaite and likasite, Miner. Mag. 74 (2010) 433-440.

[52] S. Bracci, A. Cagnini, M.P. Colombini, O.A. Cuzman, F. Fratini, M. Galeotti, D. Magrini, R. Manganelli del Fà, S. Porcinai, S. Rescic, C. Riminesi, B. Salvadori, A. Santagostino Barbone, P. Tiano, A multi-analytical approach to monitor three outdoor contemporary artworks at the Gori Collection (Fattoria di Celle, Santomato, Pistoia, Italy), Microchem. J. 124 (2016) 878–888.

[53] L. Svečnjak, G. Baranović, M. Vinceković, S. Prđun, D. Bubalo, I. Tlak Gajger, An Approach for Routine Analytical Detection of Beeswax Adulteration Using FTIR-ATR Spectroscopy, J. Apic. Sci. 59 (2015) 37–49.

[54] Y.J. Yang, S. Hu, A facile electrochemical synthesis of covellite nanomaterials at room temperature, J. Solid State Electrochem. 12 (2008) 1405–1410.

[55] G. Kalimuldina, I. Taniguchi, Electrochemical characterization of non-stoichiometric Cu_2S_x cathode for lithium batteries, J. Solid State Electrochem. 21 (2017) 3057–3063.

[56] M. Bouchard, D.C. Smith, Catalogue of 45 Raman spectra of minerals concerning research in art history or archaeology, especially on corroded metals and coloured glass, Spectrochim. Acta A 59 (2003) 2247–2266.

[57] R.L. Frost, Raman spectroscopy of selected copper minerals of significance in corrosion, Spectrochim. Acta A 59 (2003) 1195–1204.

[58] S. Jouen, M. Jean, B. Hannoyer, Simultaneous copper runoff and copper surface analysis in an outdoor area, Surf. Interface Anal. 30 (2000) 145-148.

[59] L. Robbiola, J.-M. Blengino, C. Fiaud, Morphology and mechanisms of formation of natural patinas on archaeological CuSn alloys, Corr. Sci. 40 (1998) 2083–2111.

[60] L. Robbiola, R. Portier, A global approach to the authentication of ancient bronzes based on the characterization of the alloy–patina–environment system, J. Cult. Herit.7 (2006) 1–12.

[61] A. Doménech-Carbó, M.T. Doménech-Carbó, I. Martínez-Lázaro, Layer-by-layer identification of copper alteration products in metallic works of art using the voltammetry of microparticles approach, Anal. Chim. Acta 610 (2010) 1–9.

[62] A. López-Delgado, E. Cano, J. M. Bastidas, F. A. López. A laboratory study of the effect of acetic acid vapor on atmospheric copper corrosion. J. Electrochem. Soc., 145 (1998) 4140-4147.

[63] J. M. Bastidas, A. López-Delgado, E. Cano, J. L. Polo y F. A. López. Copper corrosion mechanism in the presence of formic acid vapor for short exposure times. J. Electrochem. Soc., 147 (2000) 999-1005.

[64] A. Doménech-Carbó, M.T. Doménech-Carbó, J. Redondo-Marugán, L. Osete-Cortina, M.V. Vivancos-Ramón, Electrochemical characterization of corrosion products in leaded bronze sculptures considering ohmic drop effects on Tafel analysis, Electroanalysis 28 (2016) 833–845.

Figures

Figure 1. SWVs of sample modified-graphite electrodes immersed into air-saturated 0.25 M HAc/NaAc aqueous solution at pH 4.75 for patina 108. Potential scan initiated at a) 0.65 V in the negative direction; b) –0.85 V in the positive direction; potential step increment 4 mV; square wave amplitude 25 mV; frequency 5 Hz.

Figure 2. SWVs of sample modified-graphite electrodes immersed into air-saturated 0.25 M HAc/NaAc aqueous solution at pH 4.75 for two nitrate patinas. a,b) bb N1; c,d) bb N2. Potential scan initiated at a,c) 0.65 V in the negative direction; b,d) –0.85 V in the positive direction; potential step increment 4 mV; square wave amplitude 25 mV; frequency 5 Hz.

Figure 3. SWVs of graphite electrodes modified with patina 206: a,b) pristine and c,d) after wax treatment, immersed into air-saturated 0.25 M HAc/NaAc aqueous solution at pH 4.75. Potential scan initiated at a,c) 0.65 V in the negative direction; b,d) –0.85 V in the positive direction; potential step increment 4 mV; square wave amplitude 25 mV; frequency 5 Hz.

Figure 4. ATR-FTIR spectra of a) sample 206 without finishing; b) sample 206 after finishing with wax.

Figure 5. SWVs of graphite electrodes modified with sample db in contact with air-saturated 0.25 M HAc/NaAc aqueous solution at pH 4.75 (three replicate experiments). Potential scan initiated at a) 0.65 V in the negative direction; b) –0.85 V in the positive direction; potential step increment 4 mV; square wave amplitude 25 mV; frequency 5 Hz.

Figure 6. CVs of graphite electrodes modified with sample 605 immersed into air-saturated 0.25 M HAc/NaAc aqueous solution at pH 4.75. Potential scan initiated at 0.25 V in the negative direction and scanned between 0.65 V and: a) –0.85 V and b) –0.25 V. Potential scan rate 50 mV s^{-1}.

Figure 7. a) Scheme for the sampling with a cylindrical graphite bar of radius *r*

extracting a layer of thickness *z* on the metal patina in VIMP experiments. b) Secondary electron image of a graphite bar after sampling onto the patina 108 showing several laminas of metal patina adhered to the irregular graphite layers.

Figure 8. SWVs of sample modified-graphite electrodes immersed into air-saturated 0.25 M HAc/NaAc aqueous solution at pH 4.75 for a) nitrate patina 108, and b) chloride patina 6L. Five voltammograms after sampling with different pressures are superimposed for each patina. Potential scan initiated at 0.65 V in the negative direction; potential step increment 4 mV; square wave amplitude 25 mV; frequency 5 Hz.

Figure 9. Variation of $i(C_{1a})/i(C_{1b})$, on $i(C_{1tot})$ for cuprite (108, squares), nitrate (201, solid squares), sulfide (605, triangles), and chloride (6L, solid triangles) patinas from experiments such as in Fig. 8. Continuous lines represent the fit of experimental data to Eq. (18) using the parameter values listed in Table 2.

Figure 10. Two-dimensional diagram showing the values of the slope (*SL*) and the ordinate at the origin (*OO*) of Tafel plots determined from replicate experiments in nitrate-, sulfide-, chloride plus sulfate- based and cuprite-based artificial patinas in this study.

Table 1. Manufacturing protocols and composition of the studied historical patinas prepared in the laboratory following traditional recipes and commercial ones from Fonderia Battaglia[a] (Milan, Italy).

Code	**Substrate**	**Name (color)**	**Reagents**	**Main component of the patina (FTIR)**
108[a]	Bronze A	Claire red	$CuSO_4$, K_2SO_4	cuprite
201[a]	Bronze A	Messina green	$Cu(NO_3)_2$, $(NH_4)_2S$	gerardhtite
206[a]	Bronze A	Smalt green	$Cu(NO_3)_2$	gerardhtite
210[a]	Bronze A	Olive green	$Cu(NO_3)_2$, $FeCl_3$	gerardhtite
213[a]	Bronze A	Saint olive green	$(NH_4)_2S$	gerardhtite
605[a]	Bronze A	Medium black	$(NH_4)_2S$	covellite plus chalcocite
db	Bronze B	Dark brown	K_2S	covellite plus chalcocite
2L, 4L, 6L, 8L	Bronze B	Green	CuCl, $CuCl_2 \cdot 2H_2O$ $CuSO_4 \cdot 5H_2O$	atacamite plus brochantite
bb N1	Bronze B	Green	NH_4Cl	gerardhtite
bb N2	Bronze B	Green	NH_4Cl	gerardhtite plus covellite plus chalcocite
Bb N3	Bronze B	Green	NH_4Cl	gerardhtite plus covellite plus chalcocite
1.4	Copper	Green	$CuSO_4 \cdot 5H_2O$	brochantite
1.72	Copper	Green	$CuCO_3$, NH_3	copper(II) carbonate
1.117	Copper	Green	$NaClO_3$, $Cu(NO_3)_2$	gerardhtite

Table 2. Parameters corresponding to the fit of experimental voltammetric data to Eq. (17) for artificial patinas 108 (cuprite type), 201 (nitrate type), 605 (sulfide type), and 6L (chloride type). The densities of the corresponding mineral forms, cuprite (6.0 g cm^{-3}), gerhardtite (3.4 g cm^{-3}), covellite (4.7 g cm^{-3}), and atacamite (3.8 g cm^{-3}) have been taken as a reference in each case.

Patina	ρ_a^{sup} / g cm^{-3}	ρ_b^{inf} / g cm^{-3}	$\frac{1}{Ng_1\pi r^2\rho_b^{inf}(1+\alpha)z_o^{\alpha}}$	$\frac{1}{Ng_1\pi r^2\rho_b^{inf}(1+\beta)z_o^{\beta}}$	α	β
108	3.7	6.0	0.021	0.020	1.10	1.20
201	1.5	1.9	0.030	0.032	1.10	1.05
605	2.7	4.7	0.012	0.010	1.1	1.2
6L	1.4	3.8	0.011	0.010	1.10	1.20

Authors' contribution:

ADC conceived the research, developed the theoretical model and wrote the manuscript; BRB and CP performed electrochemical and spectroscopic measurements; SG, EC and TDC contributed to planning and writing of the manuscript.

The authors declare no competing interest.

Highlights:

* The voltammetry of immobilized particles methodology was used to study artificial patinas on copper and bronze.

* Carbonate-, nitrate-, chloride-, sulfate-, and sulfide-based patinas are characterized by their voltammetric signatures.

* In depth variation of the composition and compactness/crystallinity of the patinas is acquired.

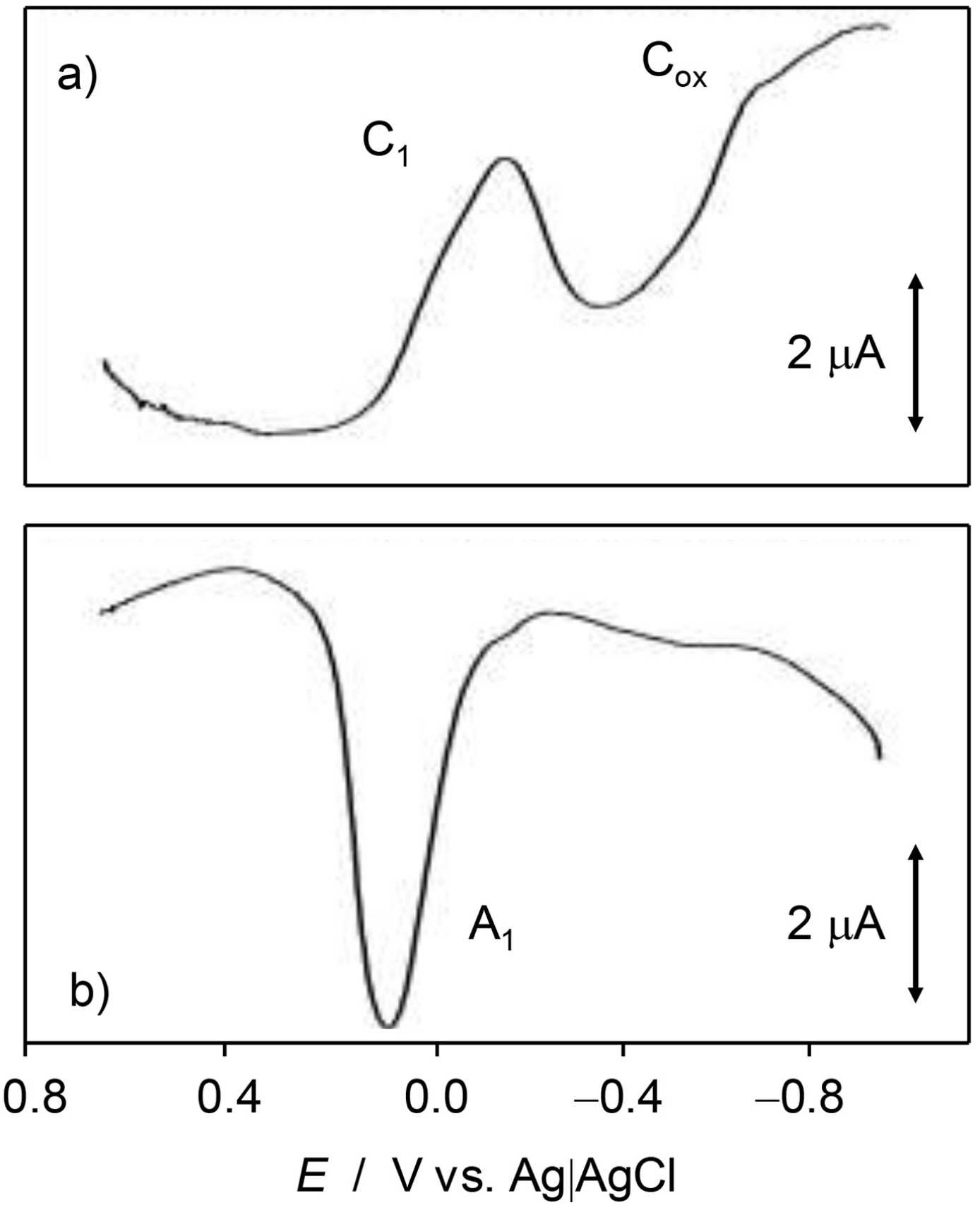

Figure 1

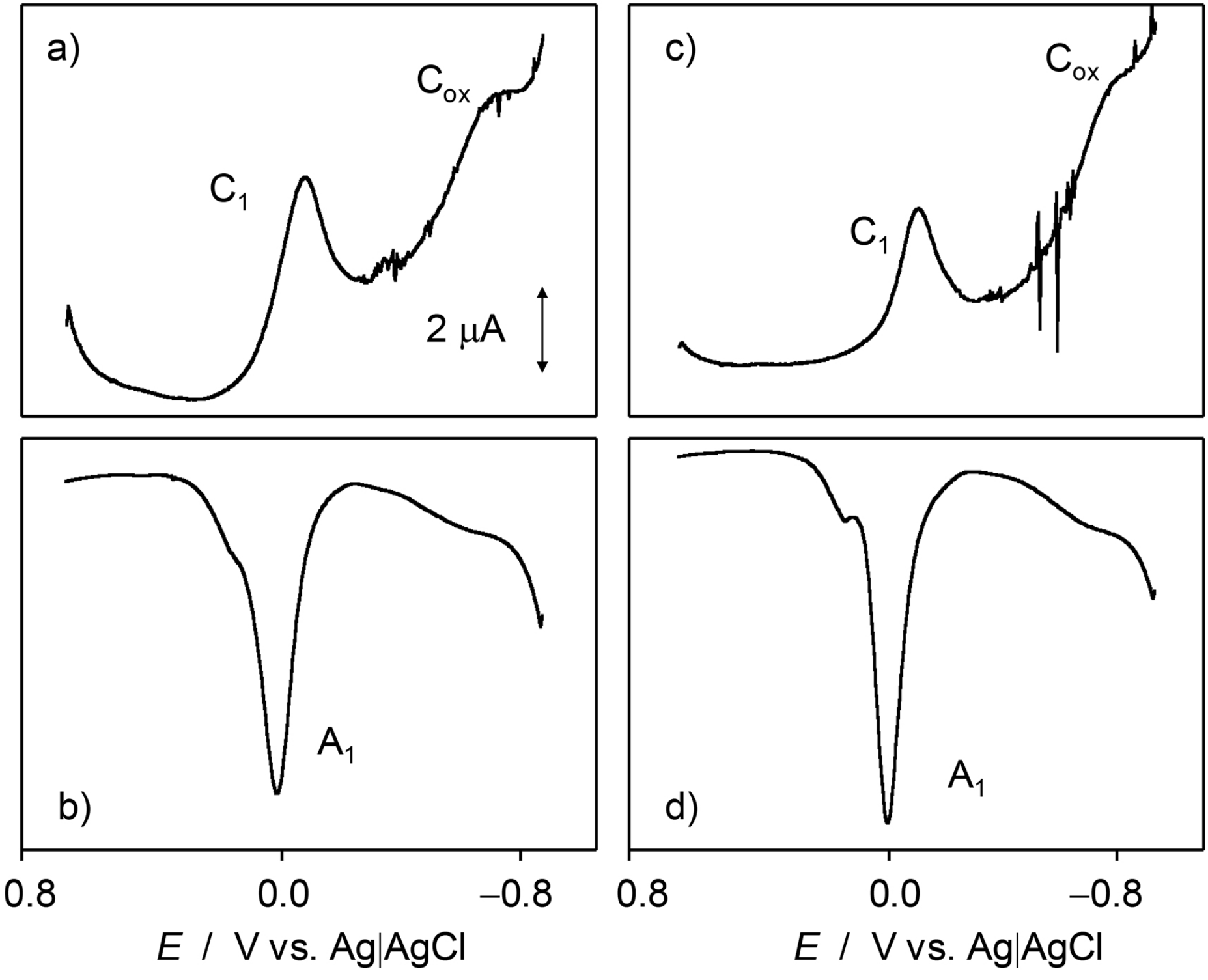
a)
C_{ox}
C_1
2 μA
c)
C_{ox}
C_1
b)
A_1
d)
A_1
0.8
0.0
–0.8
E / V vs. Ag|AgCl
0.8
0.0
–0.8
E / V vs. Ag|AgCl

Figure 2

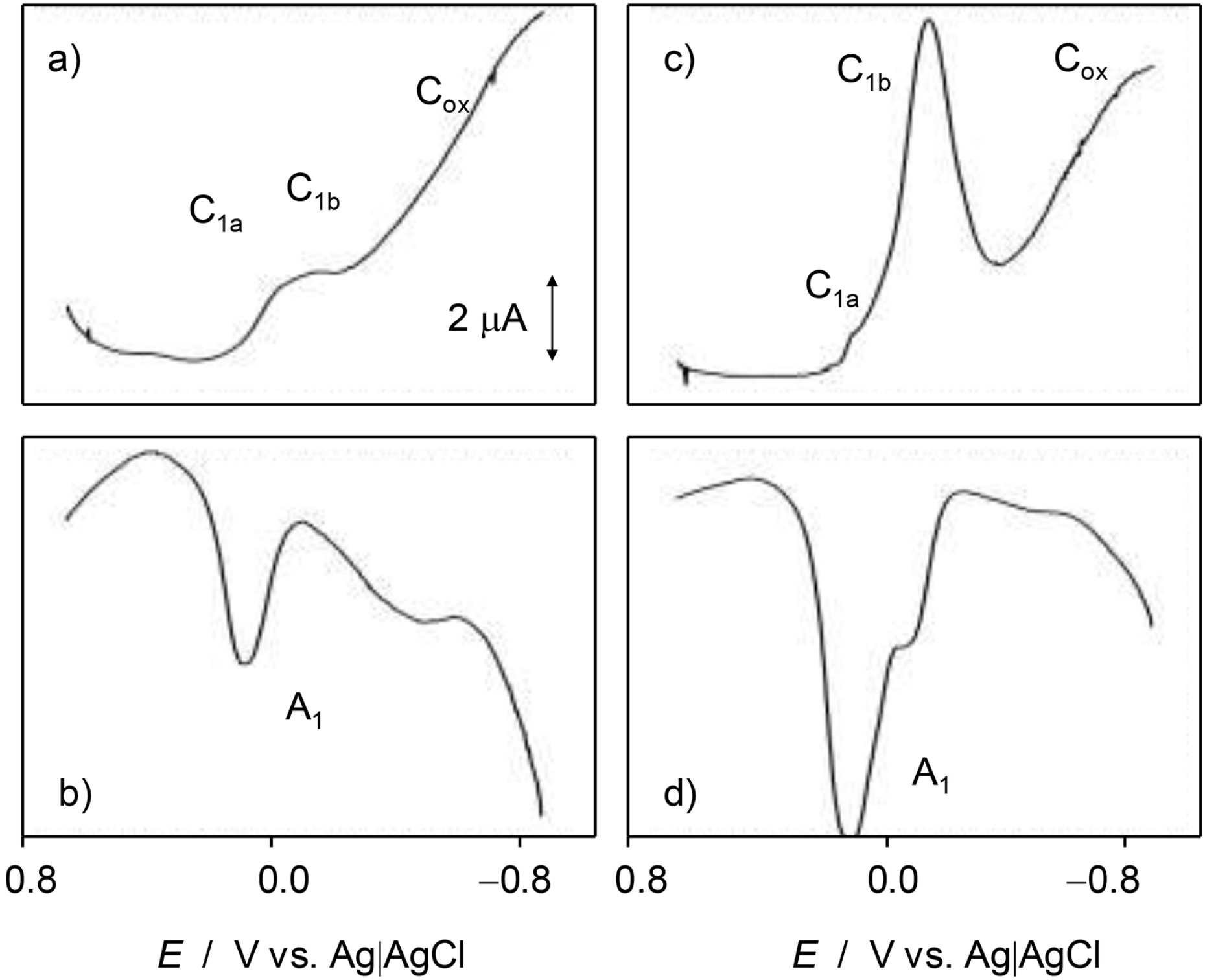
a)
C_{ox}
C_{1b}
C_{1a}
2 μA
c)
C_{1b}
C_{ox}
C_{1a}
b)
A_1
d)
A_1
0.8
0.0
−0.8
0.8
0.0
−0.8
E / V vs. Ag|AgCl
E / V vs. Ag|AgCl

Figure 3

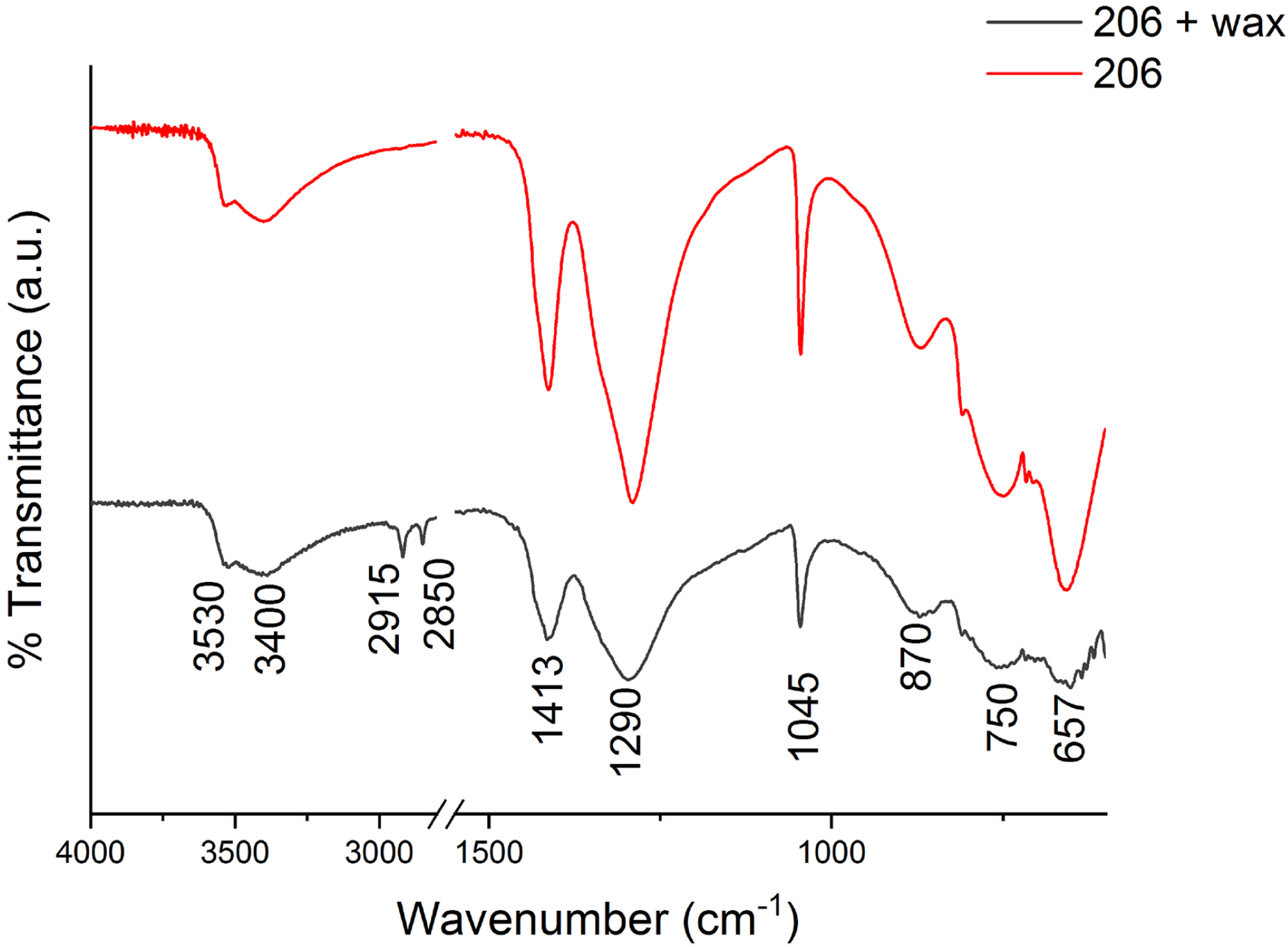
206 + wax
206
% Transmittance (a.u.)
3530
3400
2915
2850
1413
1290
1045
870
750
657
4000
3500
3000
1500
1000
Wavenumber (cm-1)

Figure 4

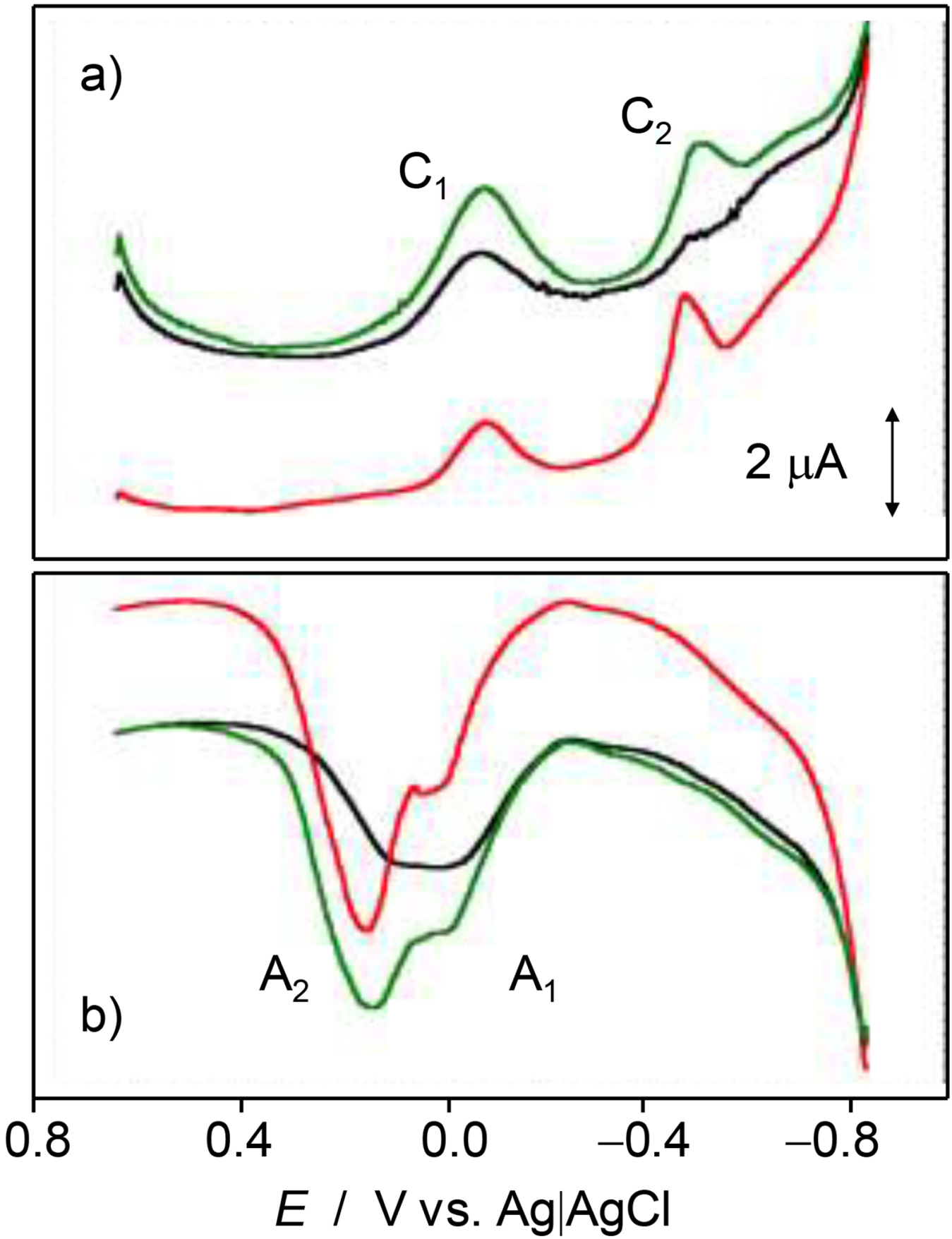

Figure 5

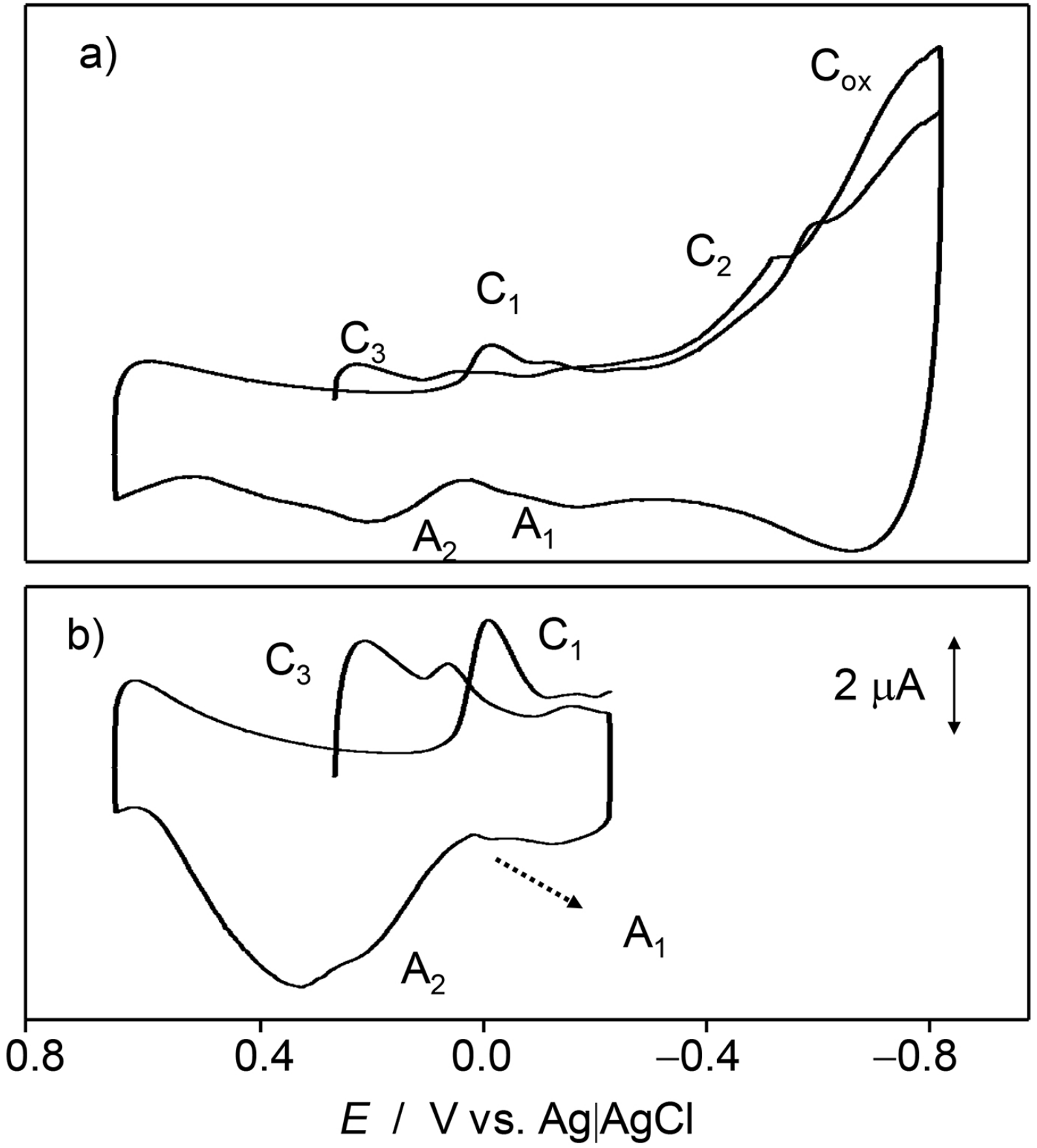

Figure 6

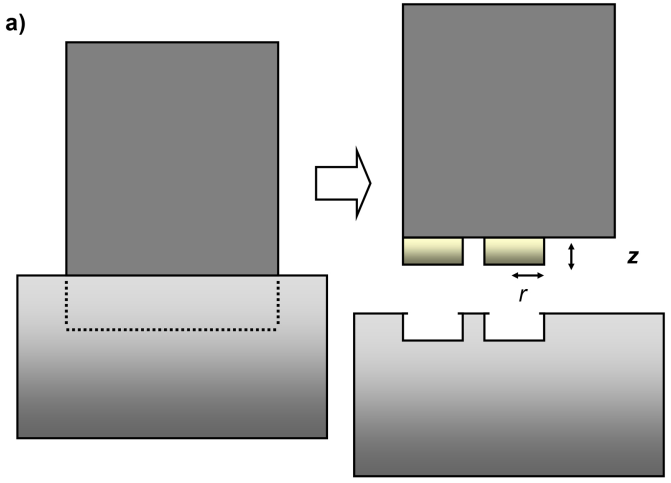

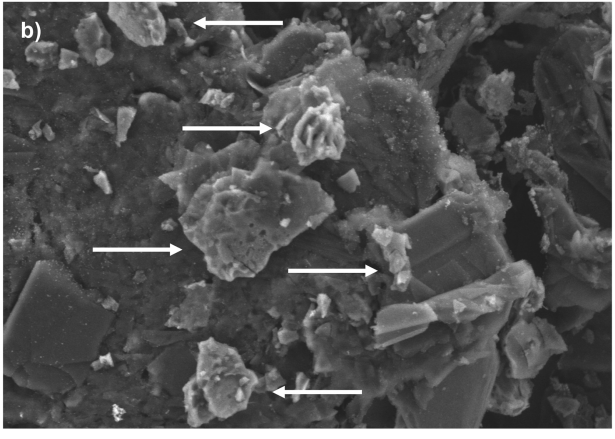

Figure 7

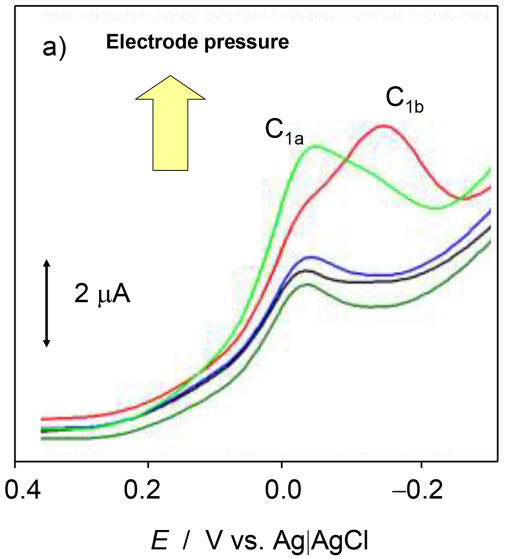
a)
Electrode pressure
C1b
C1a
2 μA
0.4
0.2
0.0
–0.2
E / V vs. Ag|AgCl

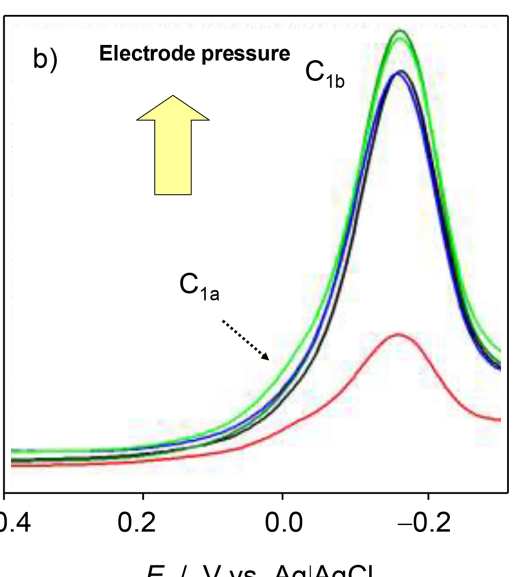
b)
Electrode pressure
C1b
C1a
0.4
0.2
0.0
–0.2
E / V vs. Ag|AgCl

Figure 8

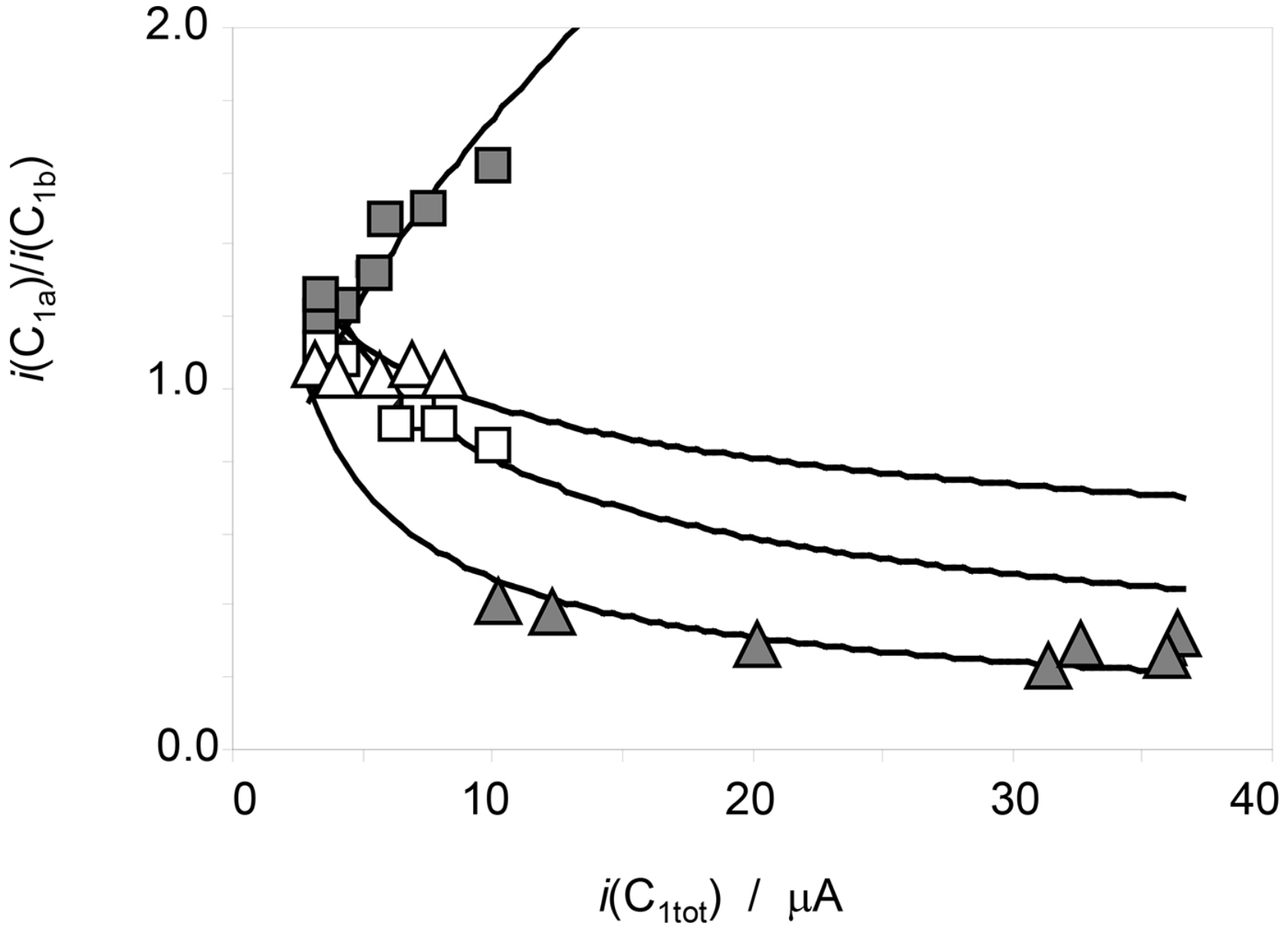

Figure 9

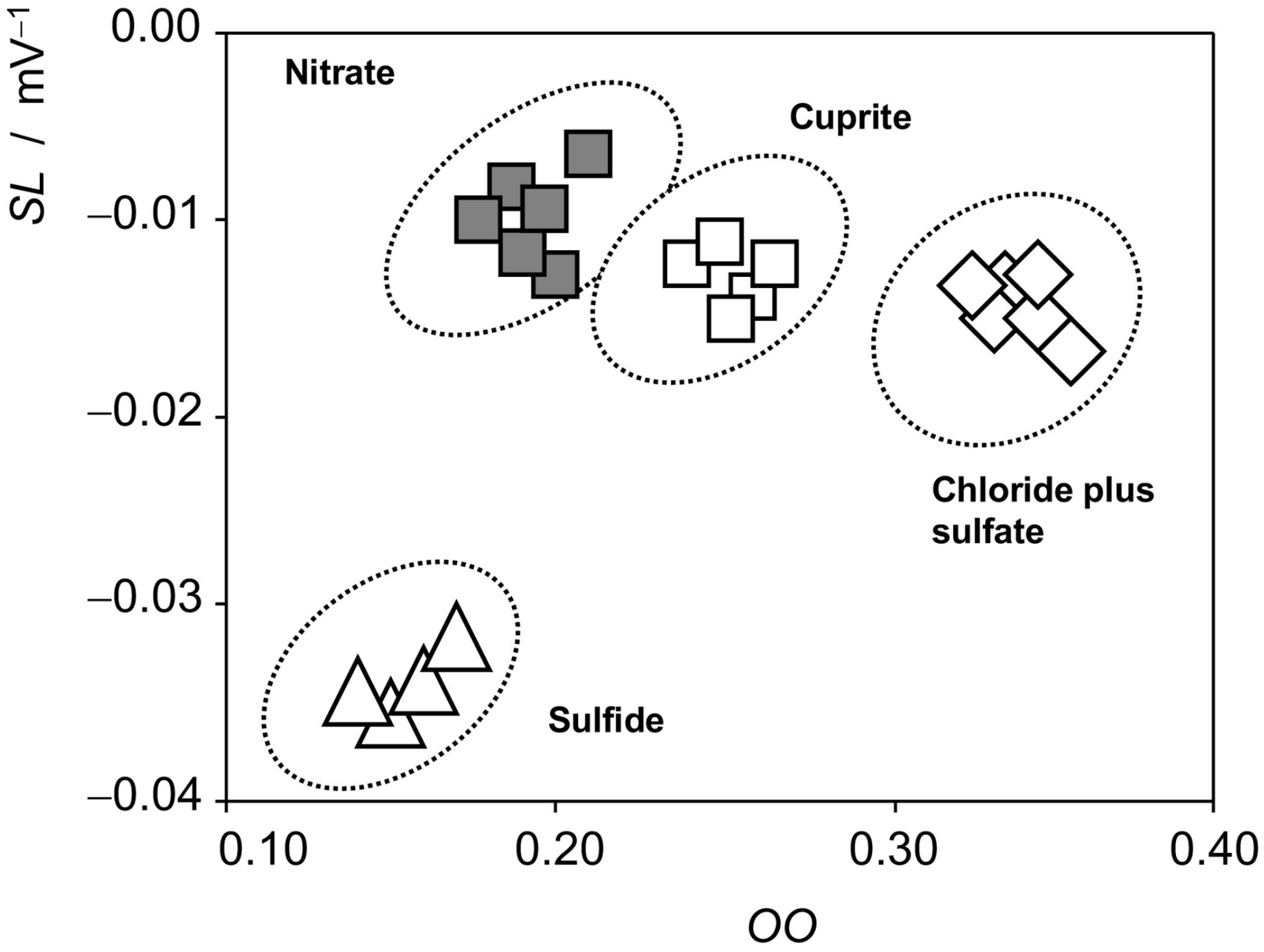
0.00
–0.01
–0.02
–0.03
–0.04
SL / mV–1
Nitrate
Cuprite
Chloride plus sulfate
Sulfide
0.10
0.20
0.30
0.40
OO

Figure 10